

Magnetic Field Evolution in Accreting White Dwarfs

Andrew Cumming*

Department of Astronomy and Astrophysics, University of California, Santa Cruz, CA 95064, USA
email: cumming@ucolick.org

2 December 2024

ABSTRACT

We discuss the evolution of the magnetic field of an accreting white dwarf. We calculate the ohmic decay modes for accreting white dwarfs, whose interiors are maintained in a liquid state by compressional heating. We show that the lowest order ohmic decay time is $(8\text{--}12) \times 10^9$ yrs for a dipole field, and $(4\text{--}6) \times 10^9$ yrs for a quadrupole field. We compare the timescales for ohmic diffusion and accretion at different depths in the star, and, under simplifying assumptions about the field structure and assuming spherical accretion, study the time-dependent evolution of the global magnetic field at different accretion rates. We neglect mass loss by classical nova explosions and assume the white dwarf mass increases with time. In this case, we find the field structure in the outer layers of the white dwarf is significantly modified for accretion rates above the critical rate $\dot{M}_c \approx (1\text{--}5) \times 10^{-10} M_\odot \text{ yr}^{-1}$. We consider the implications of our results for observed systems. We propose that accretion-induced magnetic field evolution provides the missing evolutionary link between AM Her systems and intermediate polars. The shorter ohmic decay time for accreting white dwarfs provides a partial explanation of the lack of accreting systems with $\approx 10^9$ G fields. We point out that in rapidly accreting systems such as supersoft X-ray sources, the internal magnetic field is amplified by compression, with possible implications for Type Ia supernova ignition and explosion. Finally, spreading matter in the polar cap may induce complexity in the surface magnetic field, and explain why the more strongly accreting pole in AM Her systems has a weaker field. We conclude with speculations about the field evolution when classical nova explosions cause the white dwarf mass to decrease with time.

Key words: accretion, accretion disks — stars: evolution — stars: interiors — stars: magnetic fields — white dwarfs

1 INTRODUCTION

There are now about 65 isolated magnetic white dwarfs known, and 90 accreting magnetic white dwarfs (see Wickramasinghe & Ferrario 2000, hereafter WF, for a recent review). Interesting differences are emerging between these two populations. Measured field strengths of the isolated WDs range from 3×10^4 G to 10^9 G, whereas the range of field strengths of accreting WDs may be smaller. The magnetic field strengths in the AM Her binaries are directly measured to be in the range $10^7\text{--}2 \times 10^8$ G (WF), and the magnetic fields of the intermediate polars (IPs) are inferred to range from 10^7 G down to $\approx 10^5$ G. The observed fraction of magnetic systems is 5% for isolated WDs, but 25% for accreting systems. The mean mass of isolated magnetic white dwarfs is thought to be $\gtrsim 0.95 M_\odot$, whereas measurements of accreting white dwarf masses give values $\approx 0.7 M_\odot$, consistent with non-magnetic ($B \lesssim 10^5$ G) accreting WDs.

One similarity is that the fields of both isolated and accreting objects are often seen to be complex, with a significant quadrupole (or offset dipole) component.

The origin and evolution of white dwarf magnetism is an important, but as yet unsolved, part of our understanding of stellar evolution. Several papers have discussed the evolution of magnetic fields in isolated, cooling white dwarfs. Ohmic decay of magnetic fields was first addressed by Chamugam & Gabriel (1972), and Fontaine, Thomas, & van Horn (1973), who showed that the decay time of the lowest order decay eigenmodes was longer than the evolutionary time of the white dwarf. Wendell, van Horn, & Sargent (1987; hereafter WVS) followed the evolution of different decay modes along a cooling sequence. They found that the fundamental dipole mode decayed by a factor of two in 10^{10} years. These studies suggested that WD magnetic fields are fossil fields left over from previous evolution. For example, one proposal consistent with the high masses ($\gtrsim 0.95 M_\odot$) of magnetic white dwarfs is that they result from evolution of the strongly magnetic ($10^2\text{--}10^4$ G) Ap and

* Hubble Fellow

Bp main sequence stars. The higher order field components decay more rapidly, however, leading Muslimov, van Horn, & Wood (1995, hereafter MVW) to study the Hall effect as a way to generate field complexity during the lifetime of the white dwarf.

The result that white dwarf magnetic fields evolve only very slightly over their lifetime has been applied in almost all studies of accreting white dwarfs. For example, in evolutionary studies of magnetic cataclysmic variables, it is presumed that the magnetic field of the white dwarf does not change with time. One exception is King (1985), who applied the results of Moss (1979) to accreting systems, and suggested that meridional currents could submerge magnetic flux in the outer layers of rotating magnetic white dwarfs. It is the purpose of this paper to show that the process of accretion itself may significantly change the surface magnetic field of an accreting white dwarf.

Many authors have studied the effects of accretion on the magnetic field of accreting neutron stars. This is motivated by the idea that the rapidly rotating millisecond radio pulsars are produced by accretion, which both spins up the neutron star to short periods, and somehow causes a reduction in magnetic field strength from the 10^{12} G fields seen in most radio pulsars to the 10^8 – 10^9 G fields of the millisecond pulsars (see Bhattacharya 1995 for a review). In a recent paper, Cumming, Zweibel, & Bildsten (2001; hereafter CZB) returned to the suggestion that the accretion flow directly screens the internal magnetic field (Romani 1990, 1995). They compared the timescales for ohmic diffusion and accretion in the thin outer layers of the neutron star, and computed steady-state magnetic profiles, taking the field to be horizontal and the accreted matter to be unmagnetized. For this simplified geometry, the field was found to be strongly screened for accretion rates greater than the critical rate $\dot{M} \sim 10^{-10} M_{\odot} \text{ yr}^{-1}$, whereas at lower accretion rates, the underlying magnetic field was able to penetrate the freshly accreted material. This result fits nicely with the observation that the only weakly-magnetic accreting neutron star to show its magnetic field directly (the accreting millisecond X-ray pulsar, SAX J1808.4-3658; Wijmans & van der Klis 1998; Chakrabarty & Morgan 1998) has a lower accretion rate than other systems (time-averaged $\dot{M} \approx 10^{-11} M_{\odot} \text{ yr}^{-1}$), low enough that screening would not be effective in hiding its field.

A crucial question for the evolution of accreting white dwarfs is whether the white dwarf mass increases or decreases with time. For accretion rates $\lesssim 10^{-7} M_{\odot} \text{ yr}^{-1}$, the accreted hydrogen and helium burns unstably, giving rise to classical nova explosions (e.g., see Fujimoto 1982; MacDonald 1983). The observed heavy element enrichment of nova ejecta has been used to argue that the nova explosion excavates material from the white dwarf, so that its mass is decreasing with time (e.g., Livio & Truran 1992). In addition, mixing of extra CNO nuclei into the burning shell is needed to achieve rapid enough energy release to drive novae with rapid rise times. However, this is a somewhat open question, both because of uncertainty in measurements of ejecta masses, and in theoretical modelling, particularly of the mixing between the core and accreted envelope. In recent hydrodynamic simulations of novae including diffusion, Prialnik and Kovetz (1995) found that the white dwarf mass decreased for $\dot{M} < 10^{-9} M_{\odot} \text{ yr}^{-1}$, and increased for

$\dot{M} > 10^{-7} M_{\odot} \text{ yr}^{-1}$. At intermediate accretion rates, the mass loss depends on the white dwarf temperature. The accretion rates of IPs are estimated to be $\sim 10^{-9} M_{\odot} \text{ yr}^{-1}$ (see discussion in §5.1), and their core temperatures in the middle of the range considered by Prialnik and Kovetz (1995) (see §3.2). On the other hand, AM Her systems accrete at typical rates $\approx 5 \times 10^{-11} M_{\odot} \text{ yr}^{-1}$ (§5.1). Thus a range of behaviour might be expected within the population of accreting magnetic white dwarfs. The magnetic field of the white dwarf itself may affect the nova outburst, for example by enhancing mass loss in the equatorial plane (Livio, Shankar, & Truran 1988; Livio 1995).

In this paper, we assume that the white dwarf mass *increases* with time during accretion, and study the consequences for the evolution of the white dwarf magnetic field. We leave the case of decreasing white dwarf mass for a future study. We first show that comparing accretion and ohmic diffusion times in white dwarfs gives the same critical accretion rate $\dot{M}_c \approx (1-5) \times 10^{-10} M_{\odot} \text{ yr}^{-1}$ as found for neutron stars by CZB (for reasons we describe in §3), and then go on to calculate the evolution of the magnetic field. We show that the resulting field evolution may explain several properties of observed systems.

A complication in calculating the evolution of the magnetic field in both accreting neutron stars and white dwarfs is that the accretion flow is channelled onto the magnetic polar cap (for white dwarfs, this occurs for $B \gtrsim 10^5$ G). Rather than tackle the complex problem of the subsequent spreading of matter and evolution of the magnetic field, CZB presumed that the neutron star magnetic field was buried by the accretion flow into a flattened configuration, and then used a plane-parallel model to ask what accretion rate was needed to keep the field from reemerging by ohmic diffusion. In this paper, the simplification we make is to study the evolution of the global magnetic field *under spherical accretion*. The accreted matter is expected to spread away from the polar cap when the magnetic tension force no longer supports the hydrostatic pressure (e.g., Hameury et al. 1983), so that spherical accretion is a good approximation except in a thin layer of mass $\Delta M \lesssim 10^{-10} M_{\odot} B_7^2$ for a $0.6 M_{\odot}$ white dwarf, where $B_7 = B/10^7$ G is the surface field strength. We include the uncertainty of what happens in this thin spreading layer as an uncertainty in the surface boundary condition for the spherically accreting models (see discussion in §4.1).

We start in §2 by considering ohmic decay in accreting white dwarfs, which have liquid interiors because of compressional heating by accretion. In §3, we compare the timescales for ohmic decay and accretion, and relate our results to those of CZB. In §4, we calculate the global evolution of the field, under simplifying assumptions about its geometry, for different accretion rates. We relate our models to the recent calculations of Choudhuri & Konar (2001) for accreting neutron stars, which adopt a similar approach. We find that for $\dot{M} > \dot{M}_c$, the surface field strength is reduced by accretion because ohmic diffusion is not rapid enough to allow penetration of field into the newly accreted layers. In §5 we discuss the implications of our results for observed systems. In §6, we conclude with some speculations about magnetic field evolution in the alternative scenario of decreasing white dwarf mass with time. In the Appendix, we describe our calculations of electrical conductivity for arbitrary degeneracy.

2 OHMIC DECAY IN LIQUID WHITE DWARFS

In this section, we discuss ohmic decay of the magnetic field, neglecting the effects of accretion for now. In an accreting white dwarf, compressional heating of the core results in a central temperature $\gtrsim 10^7$ K, so that the interior is kept in a liquid state. In that case, the electrical conductivity is independent of temperature, allowing us to use simple zero-temperature white dwarf models. We calculate the ohmic decay modes following the original work of Chanmugam & Gabriel (1972), Fontaine et al. (1973), and WVS. We show that the lowest order decay mode has a decay time $\approx (8 - 12) \times 10^9$ yrs, depending on white dwarf mass.

2.1 Electrical conductivity and decay time

Ohmic decay is described by the induction equation

$$\frac{\partial \mathbf{B}}{\partial t} = -\nabla \times (\eta \nabla \times \mathbf{B}), \quad (1)$$

where $\eta = c^2/4\pi\sigma$ is the magnetic diffusivity, and σ the electrical conductivity. The associated characteristic decay timescale is $\approx 4\pi\sigma L^2/c^2$, where L the lengthscale over which \mathbf{B} changes.

The interior of an accreting white dwarf is maintained in a liquid state by compressional heating. The melting temperature T_{melt} is determined by the condition $\Gamma \approx 173$ (e.g., Farouki & Hamaguchi 1993), where $\Gamma = (Ze)^2/k_B T a$ measures the ratio of Coulomb to thermal energy. For simplicity, we write Γ for a single species of ion with charge Z , mass A and interion spacing a , giving

$$T_{\text{melt}} \approx 3 \times 10^6 \text{ K } \rho_6^{1/3} \left(\frac{Z}{7}\right)^{5/3} \left(\frac{2Z}{A}\right). \quad (2)$$

This is less than the expected interior temperature of accreting white dwarfs, which undergo compressional heating, giving core temperatures $\gtrsim 10^7$ K (Nomoto 1982).

The electrical conductivity in the liquid interior is set by collisions between the degenerate electrons and the non-degenerate ions. The conductivity is

$$\sigma = \frac{8.5 \times 10^{21} \text{ s}^{-1}}{\Lambda_{ei} \langle Z \rangle} \frac{x^3}{1+x^2}, \quad (3)$$

(e.g. Yakovlev & Urpin 1980; Itoh et al. 1983; Schatz et al. 1999), where $x = p_F/m_e c$ measures the Fermi momentum p_F of the electrons, $\Lambda_{ei} \approx 1$ is the Coulomb logarithm, and $\langle Z \rangle$ is a measure of the mean nuclear charge, given by $\langle Z \rangle = \mu_e \sum X_i Z_i^2/A_i$, with Z_i the nuclear charge, A_i the mass, and X_i the mass fraction of species i , and μ_e the mean molecular weight per electron. In terms of x , the density is $\rho = 1.9 \times 10^6 \text{ g cm}^{-3} x^3 (\mu_e/2)$.

The fact that conductivity is independent of temperature allows us to adopt simple zero-temperature white dwarf models. In the outer envelope, where the electrons are non-degenerate, the conductivity is temperature-dependent. In the Appendix, we describe a method for calculating the electrical conductivity for arbitrary degeneracy. However, the results of this section are insensitive to the conductivity in the outermost layers. We adopt pressure as the independent variable, and integrate the equations of hydrostatic balance and mass conservation outwards from the centre of the white

dwarf for an initial choice of central density. We stop the integration once the pressure falls below some fixed fraction of the central pressure, at which point the radius and mass are well-determined. We assume the composition is an equal mixture by mass of carbon and oxygen, giving $\mu_e = 2$ and $\langle Z \rangle = 7$.

Some properties of these zero-temperature white dwarfs are shown in Figure 1. We show the radius, central density, central conductivity σ_c , and ohmic time at the centre, $t_{\text{ohm}} = 4\pi R^2 \sigma_c / c^2$, as a function of white dwarf mass.

Despite the large variations in R and σ_c , the ohmic time at the centre does not depend very strongly on white dwarf mass, ranging from $(2-6) \times 10^{11}$ yrs. To see why, we note that at the centre of the white dwarf $x \gtrsim 1$, so that $\sigma \propto x \propto \rho^{1/3}$. However, if the mass-radius relation is $R \propto M^{-1/3}$, then $\rho \propto M^2$, giving $\sigma \propto M^{2/3}$. The ohmic time $t_{\text{ohm}} \propto R^2 \sigma$ is thus approximately constant with mass. As the white dwarf mass increases, the increase in conductivity is offset by the decreasing radius. Most of the variation in t_{ohm} seen in Figure 1 comes from the Coulomb logarithm (see Appendix for our calculation of Λ_{ei}).

The difference between ohmic decay times in isolated white dwarfs with liquid and solid cores has been pointed out previously, particularly by MVW. For a solid, the conductivity is set by collisions of electrons with phonons, which become more common with increasing temperature (for example, see Yakovlev & Urpin 1980; Baiko & Yakovlev 1995). An example is Figure 2 of WVS, in which both the conductivity and decay timescale are roughly constant for the first $\approx 3 \times 10^8$ years of cooling history when the core is liquid, but then increase with time as the core becomes solid and cools.

2.2 Ohmic decay modes

The ohmic time at the centre t_{ohm} is an overestimate of the time for magnetic field decay, since both the conductivity and radial lengthscale are largest at the centre. To do better, we now find the ohmic decay eigenmodes for liquid white dwarfs, following the original work of Chanmugam & Gabriel (1972), Fontaine et al. (1973), and WVS.

We assume an axisymmetric poloidal magnetic field, $\mathbf{B}(r, \theta, t) = B_r(r, \theta, t)\hat{e}_r + B_\theta(r, \theta, t)\hat{e}_\theta$ which we write in terms of a vector potential $\mathbf{B} = \nabla \times \mathbf{A}$ where $\mathbf{A} = A_\phi(r, \theta, t)\hat{e}_\phi$ (see Mestel 1999 for a useful discussion). Using the identity $\nabla \times (\hat{e}_\phi/r \sin \theta) = 0$, we find

$$\mathbf{B} = \frac{\hat{e}_\phi}{r \sin \theta} \times \nabla (r A_\phi \sin \theta), \quad (4)$$

so that the quantity $r A_\phi \sin \theta$ labels the magnetic field lines.

Rewriting equation (1), we find the time evolution of \mathbf{A} is given by

$$\frac{\partial \mathbf{A}}{\partial t} = -\eta \nabla \times \nabla \times \mathbf{A}. \quad (5)$$

We now separate A_ϕ into radial and angular pieces,

$$A_\phi(r, \theta, t) = \sum_l \frac{R_l(r, t)}{r} P_l^1(\cos \theta), \quad (6)$$

where P_l^1 is the associated Legendre function of order 1. The magnetic field components are

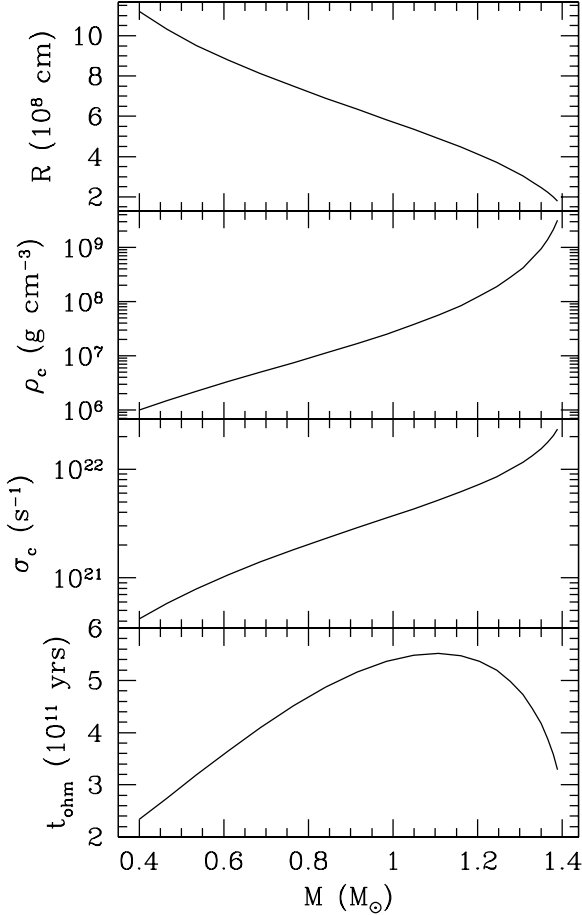


Figure 1. Properties of the zero-temperature white dwarf models. We show the radius, central density, conductivity, and ohmic time $t_{\text{ohm}} = 4\pi R^2 \sigma_c / c^2$ as a function of mass.

$$B_r = \sum_l \frac{l(l+1)}{r^2} R_l(r, t) P_l(\cos \theta) \quad (7)$$

and

$$B_\theta = - \sum_l \frac{1}{r} \frac{\partial R_l(r, t)}{\partial r} P_l^1(\cos \theta), \quad (8)$$

where P_l is the Legendre polynomial. We use spherically symmetric white dwarf models¹ in which the diffusivity depends on radius r only, and not on latitude θ . In this case, substituting equation (6) into equation (5) gives

$$\frac{\partial R_l}{\partial t} = \eta \left[\frac{\partial^2 R_l}{\partial r^2} - \frac{l(l+1)R_l}{r^2} \right], \quad (9)$$

a diffusion equation for the radial function R_l .

Neglecting mass and density changes due to accretion, the conductivity of a liquid white dwarf is independent of time, and depends only on position, $\eta(r)$. In this case, we

¹ Except in the very outermost layers, it is always a good approximation that the hydrostatic pressure P is much larger than the magnetic pressure $B^2/8\pi$.

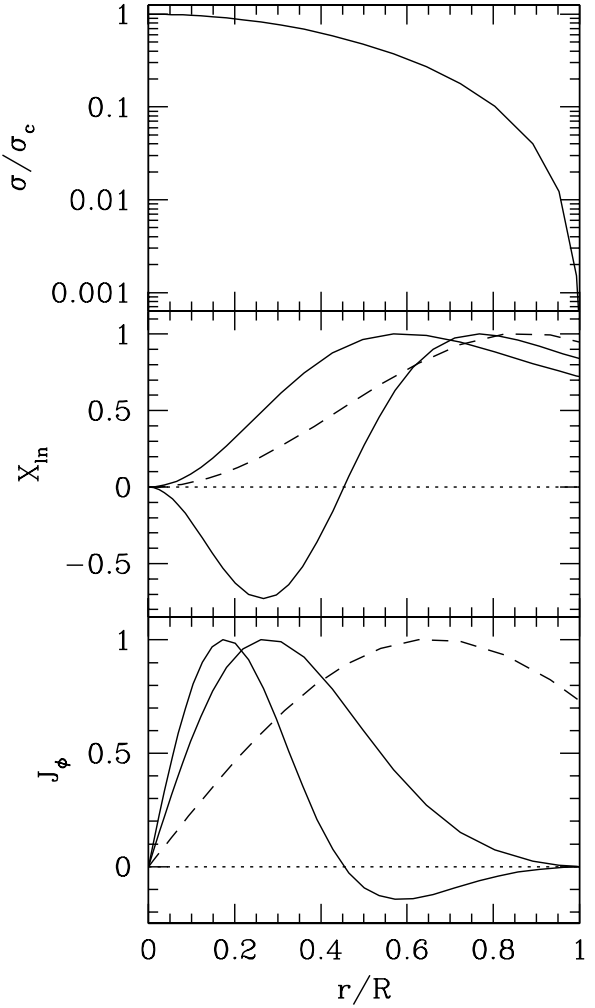


Figure 2. Ohmic decay modes for a $0.6M_\odot$ white dwarf. (i) In the upper panel, we show the conductivity as a function of radius. The central value of conductivity in this model is $\approx 10^{21} \text{ s}^{-1}$, dropping to close to the Spitzer value $\approx 5 \times 10^{17} \text{ s}^{-1}$ (eq. [19]) at the outer boundary. (ii) In the middle panel we show the $n = 1$ and 2 dipole ($l = 1$) decay modes. We normalize each eigenfunction so that its maximum value is unity. The n th mode has $(n-1)$ nodes. The dashed curve shows the $n = 1$ mode for constant conductivity with radius. (iii) The lower panel shows the distribution of current density for the eigenmodes shown in the middle panel.

follow WVS, and look for a solution which decays exponentially with decay time τ_{ln} ,

$$R_l(r, t) = \sum_n C_{ln} X_{ln}(r) \exp(-t/\tau_{ln}), \quad (10)$$

where C_{ln} is a constant giving the contribution of mode n , and the differential equation

$$\frac{d^2 X_{ln}}{dr^2} - \frac{l(l+1)X_{ln}}{r^2} + \frac{X_{ln}}{\eta(r)\tau_{ln}} = 0 \quad (11)$$

determines the eigenfunction $X_{ln}(r)$.

We adopt the following boundary conditions (see discussion in §5.6 of Mestel 1999). Inspection of equation (11)

Table 1. Ohmic decay times (τ_{ln} in units of 10^9 years)

	$M = 0.6 M_{\odot}$			$M = 1.0 M_{\odot}$		
	$(t_{\text{ohm}} = 3.4 \times 10^{11} \text{ yrs})$			$(t_{\text{ohm}} = 5.4 \times 10^{11} \text{ yrs})$		
	$n = 1$	$n = 2$	$n = 3$	$n = 1$	$n = 2$	$n = 3$
$l = 1$	7.6	2.5	1.2	12	4.1	2.0
$l = 2$	3.5	1.6	0.87	5.7	2.5	1.4
$l = 3$	2.0	1.1	0.66	3.3	1.7	1.1

shows that a finite solution at the centre of the star must have $X_{ln} \propto r^{l+1}$, giving

$$\frac{dX_{ln}}{dr} = \frac{(l+1)X_{ln}}{r} \quad r \rightarrow 0. \quad (12)$$

Outside the star, where the current $\mathbf{J} \propto \nabla \times \mathbf{B} = 0$, we choose the solution which remains finite for large r , $R_{ln} \propto r^{-l}$. Thus, we take

$$\frac{dX_{ln}}{dr} = -\frac{lX_{ln}}{r} \quad r \rightarrow R \quad (13)$$

at the surface.

Solution of equation (11) requires the conductivity as a function of radius. This is shown in the top panel of Figure 2 for a $0.6M_{\odot}$ white dwarf, normalized to the central value, $\sigma_c = 9.6 \times 10^{20} \text{ s}^{-1}$. The resulting $n = 1$ and $n = 2$ dipole ($l = 1$) decay modes X_{ln} are shown as solid lines in the middle panel of Figure 2. The lower panel shows the current density $\mathbf{J} = (c/4\pi)\nabla \times \mathbf{B}$. Using equations (5), (6), and (10), this may be written in terms of X_{ln} as $\mathbf{J} = J_{\phi} \hat{e}_{\phi}$, where

$$J_{\phi} = \frac{\sigma}{c\tau_{ln}} \left(\frac{X_{ln}}{r} \right). \quad (14)$$

Note that the n th mode has $n - 1$ nodes, the current reversing direction at a node.

Table 1 gives the decay time for modes with $l = 1, 2$ and 3 , and $n = 1, 2$, and 3 for $0.6 M_{\odot}$ and $1.0 M_{\odot}$ white dwarfs. For both white dwarf masses, we find that the lowest order decay mode ($l = 1$ and $n = 1$) has a decay time $\tau_{11} \approx t_{\text{ohm}}/40$, roughly a factor of four smaller than the analytic result for η independent of radius (in which case $\tau_{11} = t_{\text{ohm}}/\pi^2$, see WVS eq. [10]).

The decay times in Table 1 agree well with the calculations of WVS for liquid white dwarfs (compare their Figure 2). However, we do not agree with the later calculations of MVW, who report decay times an order of magnitude smaller, $(3 - 10) \times 10^8$ yrs, for liquid white dwarfs (see their §3.3), despite using the same conductive opacities for the liquid interior as WVS (see their §2.3). The origin of this difference is not clear. The central conductivity quoted by MVW for a $0.6 M_{\odot}$ white dwarf ($\approx 2 \times 10^{21} \text{ s}^{-1}$) agrees well with the value in both our models and those of WVS. In addition, changing the conductivity profile seems unlikely to give an order of magnitude change in the decay time. The difference may be due to an incorrect normalization used by MVW (H. van Horn, private communication).

To test the influence of the conductivity profile, we compared our eigenfunctions with those of WVS and MVW (Figure 3, left panel, of WVS; Figure 1, top panel of MVW). The agreement is good for times $\gtrsim 10^9$ yrs, but differs for earlier times, for which the WVS and MVW eigenfunctions peak at larger radius ($r/R \approx 0.8$ rather than $r/R \approx 0.6$). We have been unable to identify the reason for this difference. The peak at larger radius likely reflects a shallower conductivity

profile. For example, in the extreme case of constant conductivity with radius, the currents are less centrally-concentrated than in realistic models. The reason for this is that the currents flow in the regions of high conductivity; this region is more extended in the constant conductivity model. The dashed lines in the middle and lower panels of Figure 2 show the $n = 1, l = 1$ eigenmode for constant conductivity (in this case $X_{11} \propto rj_1(r)$, where j_1 is the spherical Bessel function of degree 1, see WVS). As noted above, the lowest order decay time for constant conductivity is a factor ≈ 4 longer than the realistic white dwarf models.

In summary, we find that the ohmic decay time lies in the range $\approx (8-12)$ billion years for a dipole field, and $\approx (4-6)$ billion years for a quadrupole field, depending only slightly on white dwarf mass.

3 ACCRETION VS. DIFFUSION TIMES IN THE ENVELOPE

The long timescale for ohmic decay raises the question of the effect of the accretion flow on the magnetic field structure. The decay timescale of $\approx 10^{10}$ yrs is the time to accrete the whole star at $10^{-10} M_{\odot} \text{ yr}^{-1}$. For more rapid accretion than this, one might expect the magnetic field structure to be significantly altered as the magnetic field is advected by the accretion flow.

To make a more quantitative estimate of this process, we start by comparing the timescales for accretion and diffusion across a scale height in the envelope of the white dwarf, before moving on to simple models of the global field structure in §4.

3.1 Analytic estimates

We consider the outer layers of the star, where the gravity $g = GM/R^2$ is constant. We define the column depth $y = -\int \rho dz = \Delta M/4\pi R^2$, where ΔM is the mass above column depth y . Hydrostatic balance $dP/dz = -\rho g$ becomes $dP/dy = g$, giving $P = gy$. The time to accrete the matter above a given column depth is $t_{\text{accr}} = y/\dot{m}$, where $\dot{m} = \dot{M}/4\pi R^2$ is the local accretion rate per unit area. We compare this with the ohmic diffusion time across a scale height, $t_{\text{diff}} = 4\pi\sigma H^2/c^2$.

When the electrons are degenerate, the conductivity is given by equation (3). In the outer layers, the electrons are non-relativistic, so that $P = 6.8 \times 10^{20} \text{ erg cm}^{-3} \rho_5^{5/3} (2/\mu_e)^{5/3}$. The pressure scale height is $H = P/\rho g = 6.8 \times 10^7 \text{ cm} (\rho_5^{2/3}/g_8)(2/\mu_e)^{5/3}$, giving

$$t_{\text{diff}} = 8.9 \times 10^8 \text{ yrs} \frac{\rho_5^{7/3}}{\Lambda_{ei} \langle Z \rangle g_8^2} \left(\frac{2}{\mu_e} \right)^{13/3}. \quad (15)$$

To evaluate the accretion timescale, we write the local accretion rate $\dot{m} = \dot{m}_{-3} 10^{-3} \text{ g cm}^{-2} \text{ s}^{-1}$ in terms of the global rate $\dot{M} = \dot{M}_{-10} 10^{-10} M_{\odot} \text{ yr}^{-1}$, as $\dot{m} = \dot{M}/4\pi R^2$, giving

$$\dot{m}_{-3} = 0.51 \frac{\dot{M}_{-10}}{R_9^2}. \quad (16)$$

If accretion is not occurring over the whole surface of the white dwarf, for example magnetically-controlled accretion

onto the polar caps, the relevant quantity is the local accretion rate; we work in terms of the global rate only for convenience. We find

$$t_{\text{accr}} = 4.3 \times 10^8 \text{ yrs} \frac{\rho_5^{5/3} R_9^2}{g_8 \dot{M}_{-10}} \left(\frac{2}{\mu_e} \right)^{5/3}. \quad (17)$$

The ratio of t_{diff} to t_{accr} depends on the quantity gR^2 , which we rewrite in terms of the mass of the star, $g_8 R_9^2 = 1.3(M/M_\odot)$. This gives

$$\frac{t_{\text{diff}}}{t_{\text{accr}}} = 1.6 \frac{\rho_5^{2/3} \dot{M}_{-10}}{\Lambda_{ei} \langle Z \rangle} \left(\frac{M_\odot}{M} \right) \left(\frac{2}{\mu_e} \right)^{8/3}, \quad (18)$$

which depends only weakly on depth.

Equation (18) shows that $t_{\text{diff}} \approx t_{\text{accr}}$ for accretion rates of order $10^{-10} M_\odot \text{ yr}^{-1}$. This is roughly the same critical accretion rate as found for the degenerate ocean of an accreting neutron star in CZB (compare eq. [29] of that paper). The reason is that $t_{\text{diff}}/t_{\text{accr}} \propto 1/gR^2$, so that it depends only on the mass M and not separately on the gravity and radius.

At densities $\lesssim 10^3 \text{ g cm}^{-3}$, the electrons become non-degenerate, in which case the conductivity is given by Spitzer's formula (Spitzer 1962)

$$\sigma = 7.5 \times 10^{18} \text{ s}^{-1} \frac{T_7^{3/2}}{\Lambda_{ei} \langle Z \rangle}, \quad (19)$$

where the temperature $T = T_7 10^7 \text{ K}$. For an ideal gas, the pressure scale height is $H = P/\rho g = k_B T / \mu m_p g$, where μ is the mean molecular weight, giving $H = 8.3 \times 10^6 \text{ cm } T_7 / \mu g_8$. The ohmic time is

$$t_{\text{diff}} = 2.3 \times 10^5 \text{ yrs} \frac{T_7^{7/2}}{\mu^2 g_8^2 \Lambda_{ei} \langle Z \rangle} \quad (20)$$

and the accretion time is

$$t_{\text{accr}} = 5.1 \times 10^4 \text{ yrs} \frac{T_7 \rho_2 R_9^2}{\mu g_8 \dot{M}_{-10}}. \quad (21)$$

The ratio of the two is

$$\frac{t_{\text{diff}}}{t_{\text{accr}}} = 3.3 \frac{T_7^{5/2}}{\rho_2} \frac{\dot{M}_{-10}}{\mu g_8 \Lambda_{ei} \langle Z \rangle} \left(\frac{M_\odot}{M} \right). \quad (22)$$

We have inserted typical values for temperature and density, although the exact value of this ratio depends on the T - ρ relation in the atmosphere. For a constant flux atmosphere with free-free opacity, $T \propto \rho^{4/13}$, giving $t_{\text{diff}}/t_{\text{accr}} \propto \rho^{-3/13}$, again weakly dependent on density.

3.2 Detailed models

We calculate models of the atmosphere by integrating the heat flux equation

$$F = \frac{4acT^3}{3\kappa} \frac{dT}{dy} \quad (23)$$

and the entropy equation

$$\frac{dF}{dy} = -\frac{c_P T \dot{m}}{y} \left[\nabla_{\text{ad}} - \frac{d \ln T}{d \ln y} \right], \quad (24)$$

where κ is the opacity, c_P the specific heat at constant pressure, and the adiabatic index is $\nabla_{\text{ad}} = (d \ln T / d \ln P)_{\text{ad}}$. The terms on the right of equation (24) represent the effects of

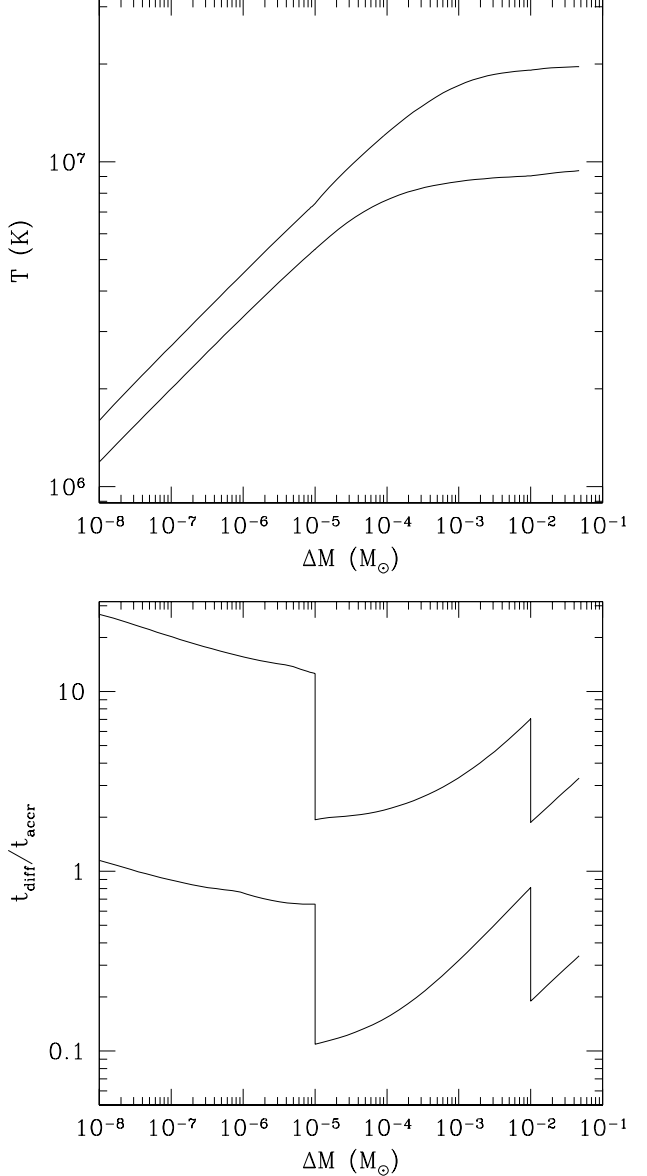


Figure 3. (i) Temperature profiles in the white dwarf envelope for $\dot{M} = 10^{-10}$ (lower curve) and $10^{-9} M_\odot \text{ yr}^{-1}$ (upper curve), for a $0.6 M_\odot$ white dwarf. (ii) Ratio of ohmic time to accretion time in the envelope for $\dot{M} = 10^{-10}$ (lower curve) and $10^{-9} M_\odot \text{ yr}^{-1}$ (upper curve). The composition is solar for $\Delta M < 10^{-5} M_\odot$, pure He for $10^{-5} M_\odot < \Delta M < 10^{-2} M_\odot$, and C/O for $\Delta M > 10^{-2} M_\odot$.

compressional heating (Nomoto 1982; Townsley & Bildsten 2001).

We integrate equations (23) and (24) from the top of the atmosphere to the base, iterating the choice of flux at the top until we match the correct flux from the core. We calculate the opacity, which includes contributions from free-free, electron scattering and conduction, as described by Schatz et al. (1999). Our calculation of electrical conductivity, which reduces to equation (3) for degenerate electrons, and equation (19) for non-degenerate electrons, is described in the Appendix.

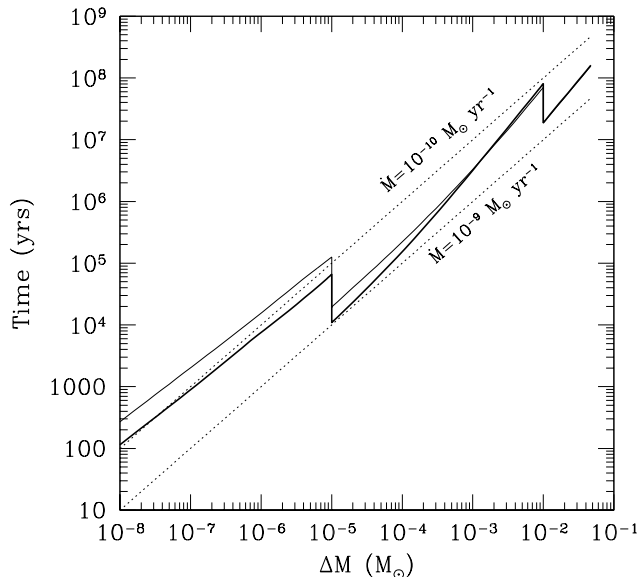


Figure 4. Ohmic diffusion time (solid lines) and accretion time (dotted lines) in the white dwarf envelope for the models of Figure 3 ($\dot{M} = 10^{-10}$ and $10^{-9} M_{\odot} \text{ yr}^{-1}$). The accretion time (dotted lines) is labelled with the appropriate accretion rate (the accretion time is smaller for a higher accretion rate). The diffusion time (solid lines) is independent of accretion rate in the degenerate layers (the conductivity depends only on density); but is longer for higher accretion rates in the non-degenerate layers (the conductivity increases with temperature).

As an illustrative model of the outer layers of an accreting white dwarf, we take a layer of solar abundance material of mass $10^{-5} M_{\odot}$, a pure helium layer of mass $10^{-2} M_{\odot}$, and a white dwarf mass of $0.6 M_{\odot}$, with an equal mixture by mass of carbon and oxygen in the core. We choose a luminosity from the core of $10^{-3} L_{\odot}$. We show the resulting temperature profiles for $\dot{M} = 10^{-10}$ and $10^{-9} M_{\odot} \text{ yr}^{-1}$ in Figure 3. For $\dot{M} = 10^{-10} M_{\odot} \text{ yr}^{-1}$, we find a core temperature 9.4×10^6 K, luminosity $4.7 \times 10^{-3} L_{\odot}$ and effective temperature 13,600 K. For $\dot{M} = 10^{-9} M_{\odot} \text{ yr}^{-1}$, we find a core temperature 2.0×10^7 K, luminosity $6.2 \times 10^{-2} L_{\odot}$ and effective temperature 25,900 K. These values are in reasonable agreement with the detailed models of compressional heating recently presented by Townsley & Bildsten (2001). A simple estimate of the compressional heating luminosity is to write

$$L \approx c_P T \dot{M} \approx 3.4 \times 10^{-3} L_{\odot} T_7 \dot{M}_{-10}, \quad (25)$$

where we use the heat capacity of an ideal gas $c_P = 5k_B/2\mu m_p$, and take $\mu \approx 1$ as a mean value in the envelope. This estimate agrees well with our numerical results.

The ratio $t_{\text{diff}}/t_{\text{accr}}$ is shown in Figure 3, and the ohmic time and accretion time individually in Figure 4. Our numerical results agree well with the analytic estimates in §3.1. In the degenerate layers ($\Delta M \gtrsim 10^{-5}$), $t_{\text{diff}}/t_{\text{accr}}$ increases with depth (eq. [18]). The jumps in $t_{\text{diff}}/t_{\text{accr}}$ at $\Delta M = 10^{-5} M_{\odot}$ and $\Delta M = 10^{-2} M_{\odot}$ result from the changes in composition from solar to pure He and from pure He to C/O (eqs. [18] and [22] give $t_{\text{diff}}/t_{\text{accr}} \propto 1/\langle Z \rangle$). At low densities, $t_{\text{diff}}/t_{\text{accr}}$ decreases with depth, as expected from equation (22).

The condition $t_{\text{diff}} = t_{\text{accr}}$ defines a critical accretion rate \dot{M}_c . Inspection of Figure 3 shows that for the accreted envelope ($\Delta M < 10^{-5} M_{\odot}$), $\dot{M}_c \approx 10^{-10} M_{\odot} \text{ yr}^{-1}$, and for the He layer and the C/O core, an average value is $\dot{M}_c \approx 5 \times 10^{-10} M_{\odot} \text{ yr}^{-1}$. This agrees well with our analytic estimates (compare eqs. [18] and [22] when $t_{\text{diff}}/t_{\text{accr}} = 1$).

4 GLOBAL MODELS OF ACCRETION AND DIFFUSION

In this section, we follow the effects of advection and diffusion in a simple model of the global magnetic field structure. We show that the evolution is very different depending on whether \dot{M} is less than or greater than the critical rate $\dot{M}_c \approx (1-5) \times 10^{-10} M_{\odot} \text{ yr}^{-1}$ found in §3.

4.1 A simple model of the global field evolution

We make the following simplifying assumptions: (i) we consider an axisymmetric, poloidal magnetic field, (ii) we assume spherical accretion, and (iii) we take the accreted matter to have the same composition as the core (equal amounts by mass of C and O). Under spherical accretion, each spherical harmonic component l evolves independently, so that an initially dipolar field remains dipolar as accretion proceeds. In reality, the accreted matter is channelled onto the polar caps in magnetic systems, subsequently spreading over the surface of the star. We do not attempt to model this process here, meaning that we must pay careful attention to our choice of surface boundary condition. We discuss this issue below, but first outline the equation describing the evolution of the magnetic field, and how we solve it.

The induction equation with advection included is

$$\frac{\partial \mathbf{B}}{\partial t} = \nabla \times (\mathbf{v} \times \mathbf{B}) - \nabla \times (\eta \nabla \times \mathbf{B}), \quad (26)$$

or, in terms of the vector potential \mathbf{A} ,

$$\frac{\partial \mathbf{A}}{\partial t} = \mathbf{v} \times (\nabla \times \mathbf{A}) - \eta \nabla \times \nabla \times \mathbf{A}. \quad (27)$$

As previously, we consider an axisymmetric field, so that $\mathbf{A} = A_{\phi}(r, \theta) \hat{e}_{\phi}$. In the absence of diffusion, equation (27) gives

$$\left(\frac{\partial}{\partial t} + \mathbf{v} \cdot \nabla \right) (r A_{\phi} \sin \theta) = 0 \quad (28)$$

(WVS; Choudhuri & Konar 2001). The quantity $r A_{\phi} \sin \theta$ (which labels the magnetic field lines, see §2.2) is advected by the poloidal velocity field.

As before, we separate A_{ϕ} into radial and angular pieces according to equation (6). We take the velocity field to be purely radial, $\mathbf{v} = v_r(r, \theta) \hat{e}_r$. Equation (27) then gives

$$\frac{\partial R_l}{\partial t} = -v_r \frac{\partial R_l}{\partial r} + \eta \left[\frac{\partial^2 R_l}{\partial r^2} - \frac{l(l+1)R_l}{r^2} \right]. \quad (29)$$

This equation governs the evolution of $R_l(r, t)$ under the joint action of accretion and diffusion.

We evolve equation (29) numerically². At each time

² This numerical approach is similar to that of WVS, who included the advection terms in their study of cooling white dwarfs.

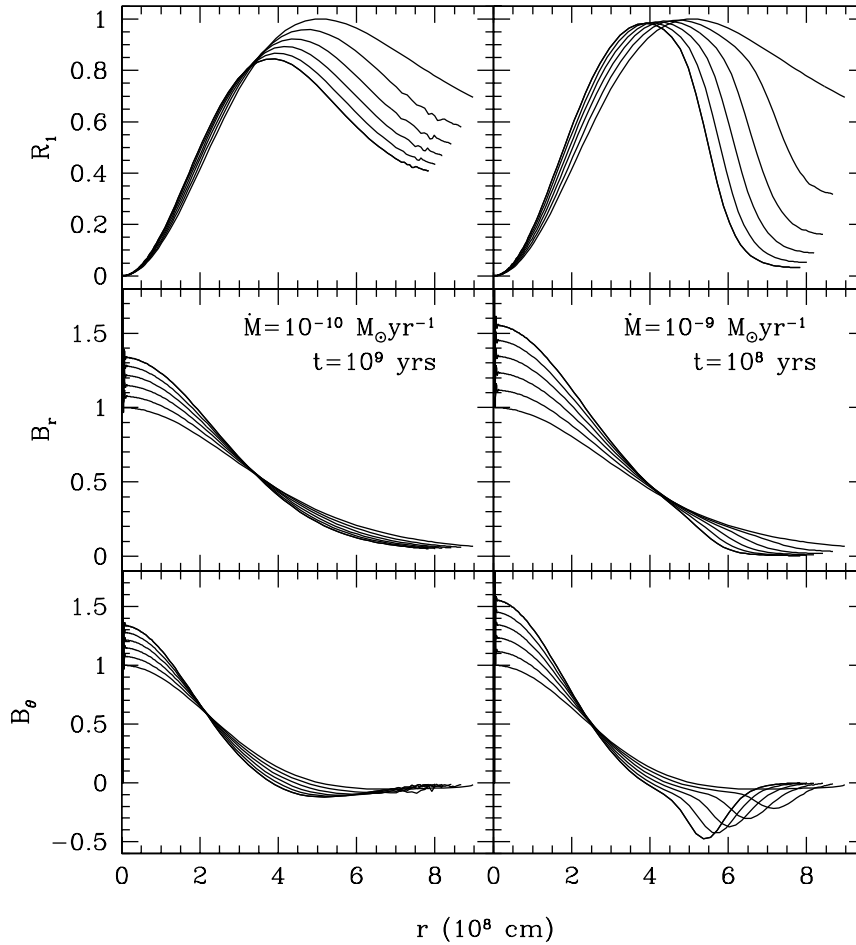


Figure 5. Time evolution of the magnetic field during accretion of $0.1 M_{\odot}$ onto a $0.6 M_{\odot}$ white dwarf. We assume “vacuum” boundary conditions (see discussion in §4.1). The left panel shows $\dot{M} = 10^{-10} M_{\odot} \text{ yr}^{-1}$, for which the accretion takes 10^9 years; the right panel shows $\dot{M} = 10^{-9} M_{\odot} \text{ yr}^{-1}$, for which the time elapsed is 10^8 years. The curves are spaced by equal increments in central density, which increases from $\approx 3 \times 10^6 \text{ g cm}^{-3}$ to $\approx 6 \times 10^6 \text{ g cm}^{-3}$. We normalise R_l to have a maximum value $R_l = 1$ initially, and normalise B_r and B_{θ} to have a central value of unity initially.

step, we include advection by making a new white dwarf model (as described in §2.1) with a slightly larger mass, but keep R_l fixed for a given fluid element. We then apply an implicit Crank-Nicholson scheme for the diffusion term (e.g. Press et al. 1992). With accretion switched off, our code accurately follows the predicted decay of the eigenmodes found in §2.

We adopt two different boundary conditions at the sur-

face. The first is the “vacuum” boundary condition given by equation (13). The second boundary condition is a “screened” boundary condition $R_l = 0$ at the surface. In the advection step, the boundary condition determines the values of R_l assigned to the newly accreted matter. As described above, we take the composition of the accreted material to be equal mass fractions of C and O. At the centre of the star, where v_r vanishes, we apply equation (12).

The “vacuum” boundary condition implies $\mathbf{J} = 0$ outside the star, as in §2, and that each shell of matter is accreted with the vacuum field at the surface. This boundary condition was adopted by Choudhuri & Konar (2001) in their recent study of accreting neutron stars (these authors solved eq. [27] with a prescribed 2D velocity field). In our 1D model, we envisage this boundary condition as approximat-

WVS found that the significant contraction which occurs in the pre-white dwarf stages of evolution increased the rate of ohmic decay, by taking the initial $n = 1$ decay mode and generating higher n components. This interesting effect is not significant during the accretion process, which involves much smaller changes in white dwarf radius.

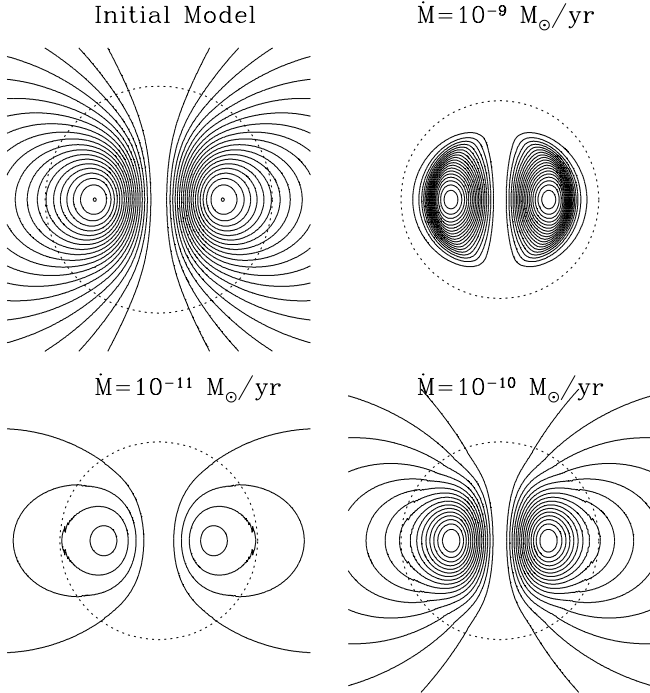


Figure 7. Magnetic field lines for the models shown in the left panel of Figure 6. We show the initial field structure in the top left panel, and the final structure for (clockwise from the top right) $\dot{M} = 10^{-9}$, 10^{-10} , and $10^{-11} M_{\odot} \text{ yr}^{-1}$. The dotted line indicates the stellar surface (note the larger radius of the less massive initial model). We show field lines with the same value of flux in each panel. The dramatic ohmic decay at the lowest accretion rate appears as the reduction in the number of field lines.

ing the case where the accreted material is able to spread away from the polar cap without significantly distorting the field structure. This is similar to Choudhuri & Konar (2001), who put in an outwards radial velocity in the outer layers to simulate the effects of buoyancy instabilities. They found the evolution of the field was then determined by advection in the interior. The “screened” boundary condition $R_l = 0$ assumes screening currents at the surface, similar in spirit to the plane parallel models of CZB for accreting neutron stars, and to the idea that the magnetic field may be completely buried by accretion.

These two different boundary conditions illustrate the range of behaviour that might be expected given a more complex flow geometry and better treatment of the outer layers, including effects such as buoyancy or interchange instabilities. In the next section, we present our numerical results. We show that the evolution of the field depends upon whether the accretion rate is above or below the critical rate \dot{M}_c .

4.2 Results

Figure 5 shows the time evolution of a dipole field during accretion of $0.1 M_{\odot}$ onto a $0.6 M_{\odot}$ white dwarf at two different accretion rates. We take a “vacuum” boundary condition, and the initial profile of $R_1(r)$ to be the lowest order dipole decay mode. We show the time evolution of R_1 ,

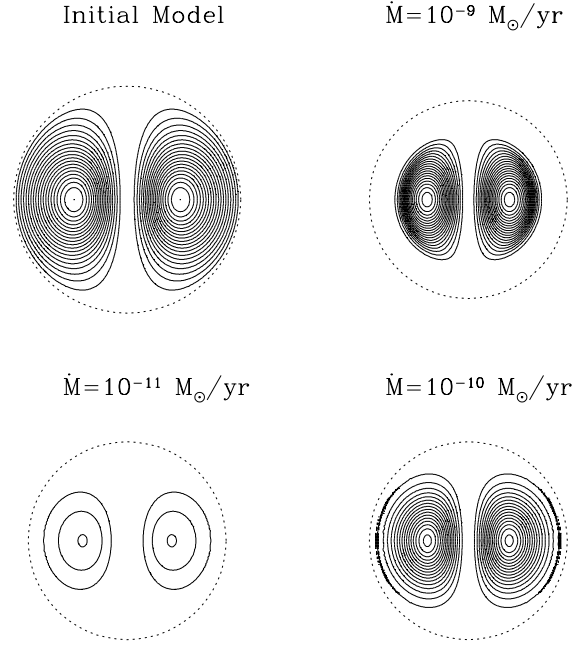


Figure 8. As Figure 7, but for the right panel of Figure 6 (screening boundary condition).

B_r ($\propto R_1/r^2$, eq. [7]), and B_{θ} ($\propto (1/r)(dR_1/dr)$, eq. [8]) at equal steps in central density. We normalize R_1 so that the initial profile has a maximum value $R_1 = 1$, and normalize B_r and B_{θ} so that the initial central value is unity. The initial central density is $\approx 3 \times 10^6 \text{ g cm}^{-3}$, increasing to $\approx 6 \times 10^6 \text{ g cm}^{-3}$. The left panel is for $\dot{M} = 10^{-10} M_{\odot} \text{ yr}^{-1}$, in which case the accretion lasts for 10^9 years, and the right panel is for $\dot{M} = 10^{-9} M_{\odot} \text{ yr}^{-1}$, in which case the accretion lasts for 10^8 years.

At $\dot{M} = 10^{-10} M_{\odot} \text{ yr}^{-1}$ (left panel of Figure 5), the magnetic field has time to diffuse into the newly accreted material. The overall decrease in R_1 is due to ohmic decay during the 10^9 years of accretion (the lowest order decay time of the initial model is $\tau_{11} = 7.6$ billion years). At $\dot{M} = 10^{-9} M_{\odot} \text{ yr}^{-1}$ (right panel of Figure 5), the accreted material is added too quickly for significant diffusion, so that the surface value of R_1 drops as accretion proceeds. The central values of B_r and B_{θ} increase by a factor of ≈ 1.6 . This can be understood in terms of the combination of flux conservation, which gives $r^2 B = \text{constant}$, and mass conservation, which gives $r^3 \rho = \text{constant}$. Eliminating r , we find $B \propto \rho^{2/3}$, giving an increase in B of 1.6 when ρ increases by a factor of 2. (In the thin layer considered by CZB, the compression was one-dimensional, giving $B \propto \rho$ in that case; see their eq. [13]).

Figure 6 shows the final magnetic profiles for accretion at several different rates. We show the profiles for vacuum boundary conditions (left panel) and screened boundary conditions (right panel). The initial profile in each case is shown by the dotted line, and is the lowest order decay mode of the initial model (subject to the respective surface boundary condition). We show accretion rates $\dot{M} = 10^{-11}$, 10^{-10} , 10^{-9} and $10^{-8} M_{\odot} \text{ yr}^{-1}$. At the lowest accretion

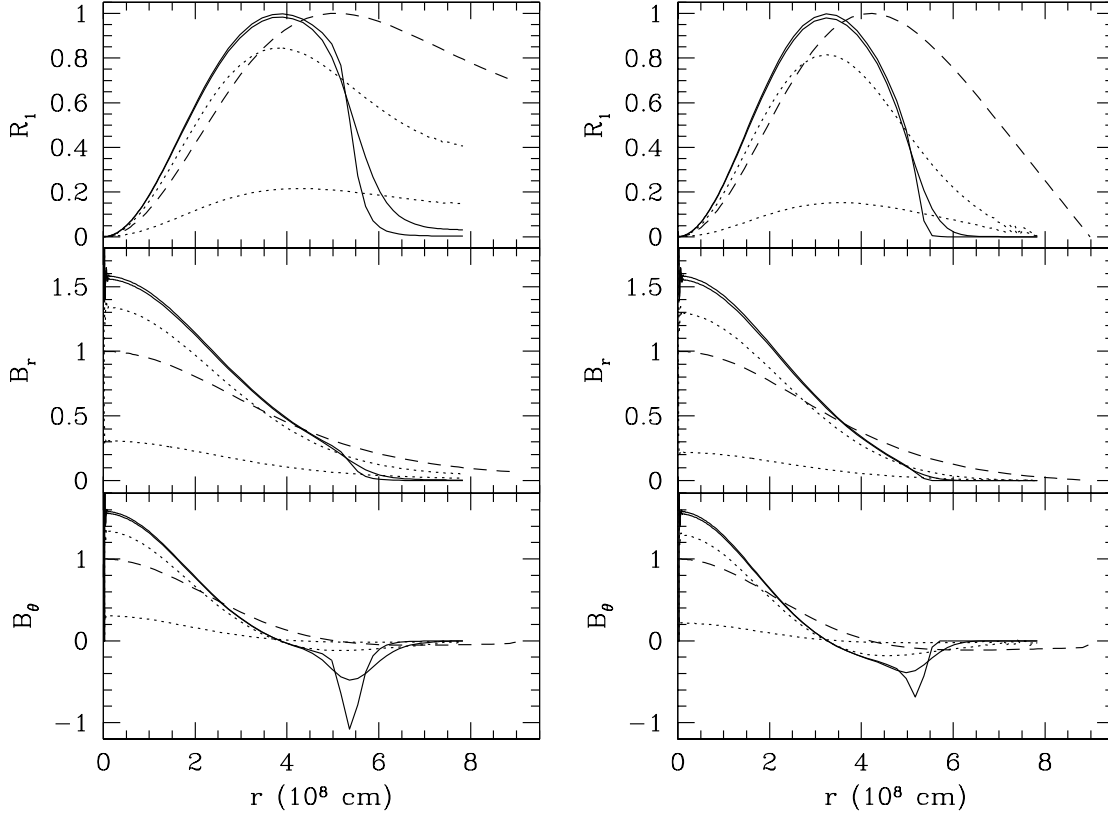


Figure 6. The profiles of R_1 , B_r , and B_θ after the accretion of $0.1 M_\odot$ onto a $0.6 M_\odot$ white dwarf at different rates. We show results for vacuum boundary conditions (left panel) and screening boundary conditions (right panel). The dashed line in each panel shows the initial state. The solid lines show accretion rates 10^{-8} and $10^{-9} M_\odot \text{ yr}^{-1}$, for which mass is accreted too rapidly to become significantly magnetised. The dotted lines show accretion rates 10^{-10} and $10^{-11} M_\odot \text{ yr}^{-1}$, for which ohmic diffusion has time to magnetise the accreted material. Significant ohmic decay of the field occurs at these low rates, because the accretion takes a long time.

rates, 10^{-11} and $10^{-10} M_\odot \text{ yr}^{-1}$ (dashed lines), the magnetic field is able to diffuse into the newly accreted layers. The decrease in R_1 is due to ohmic decay over the long timescale of accretion. For accretion rates 10^{-9} and $10^{-8} M_\odot \text{ yr}^{-1}$ (solid lines), the accreted layers do not have time to become significantly magnetized. At $\dot{M} = 10^{-8} M_\odot \text{ yr}^{-1}$, the final profile is almost exactly that given by conserving R_1 in each fluid element as accretion proceeds.

In Figures 7 and 8, we show the magnetic field lines for the profiles in Figure 6. We show field lines with the same values of $rA_\phi \sin \theta$ in each panel. The $\dot{M} = 10^{-11} M_\odot \text{ yr}^{-1}$ has only two field lines because of the significant ohmic decay that occurs as accretion proceeds. Similarly, at $10^{-9} M_\odot \text{ yr}^{-1}$, all of the field lines shown in the initial model have been pushed into the interior by the accretion flow.

Figure 9 shows R_1 , B_r , and B_θ at the surface as a function of mass accreted for a vacuum boundary condition. As we discussed §4.1, the quantitative decrease in the surface field depends on the chosen surface boundary condition. However, Figure 9 shows the qualitative effect of accretion at different rates. From top to bottom, the accretion rates are $\dot{M} = 10^{-10}$, 10^{-11} , and $10^{-9} M_\odot \text{ yr}^{-1}$. At $\dot{M} = 10^{-10} M_\odot \text{ yr}^{-1}$, the surface field changes only slightly as the newly accreted material is able to become magne-

tized by diffusion. For $\dot{M} = 10^{-11} M_\odot \text{ yr}^{-1}$, the surface field decreases due to ohmic decay (in this case the accretion takes 10^{10} years, comparable to the decay time). For $\dot{M} = 10^{-9} M_\odot \text{ yr}^{-1}$, the change is directly due to accretion.

5 IMPLICATIONS FOR OBSERVED SYSTEMS

In the previous sections, we have shown that, under the assumption that the white dwarf retains the mass it accretes, the surface magnetic field may be significantly reduced for accretion rates greater than the critical value $\dot{M}_c \approx (1-5) \times 10^{-10} M_\odot \text{ yr}^{-1}$. We now conclude by discussing the implications of our results for observed systems. We show that there are several interesting potential consequences of abandoning the assumption that the magnetic fields of accreting white dwarfs do not change with time.

5.1 An evolutionary connection between AM Hers and intermediate polars?

Accreting white dwarfs fall into two classes. Those in AM Her systems rotate synchronously with the binary orbital period, and have fields $10^7-3 \times 10^8$ G (WF). Intermediate polars (see review by Patterson 1994), in which the white

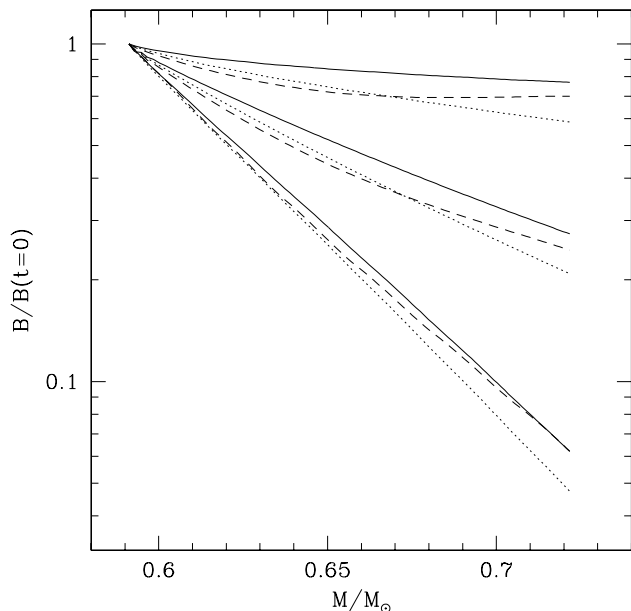


Figure 9. For the vacuum boundary condition solutions, we show surface values of R_1 (dotted line), B_r (solid line), and B_θ (dashed line) relative to their initial values as a function of white dwarf mass for (top to bottom) $\dot{M} = 10^{-10}$, 10^{-11} , and $10^{-9} M_\odot \text{ yr}^{-1}$.

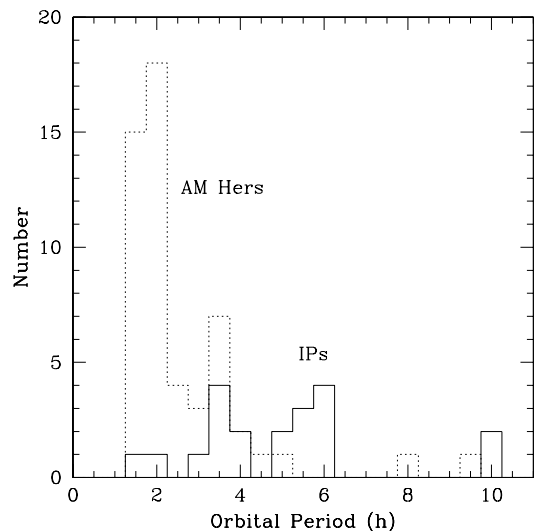


Figure 10. The orbital periods of AM Her systems and intermediate polars. We show orbital periods for 53 AM Her systems from Wickramasinghe & Ferrario (2000), and for 20 intermediate polars from the catalogue of Ritter & Kolb (1998). We exclude the intermediate polar GK Per which has $P_{\text{orb}} = 2$ days and an evolved companion.

dwarf rotates asynchronously, are believed to contain white dwarfs with fields $\sim 10^5$ – 10^7 G, although most have not been measured directly (the lower limit here is the field strength needed to disrupt the accretion flow before it hits the white dwarf surface). The asynchronous rotation of the white dwarfs in IPs lead to early suggestions that the white dwarf magnetic fields are lower than in AM Hers (for example, Lamb & Patterson 1983 estimated $B \sim 10^6$ G). In addition, whereas strong optical polarization is seen in AM Hers, little or no polarization is seen in IPs, also suggesting weaker magnetic fields. Recently, the lack of Zeeman splitting in spectroscopic observations of the white dwarf in V709 Cas (Bonnet-Bidaud et al. 2001) has constrained the magnetic field to be $< 10^7$ G.

The two classes show an interesting difference in accretion rates. AM Her systems accrete at low rates, $\dot{M} \approx 5 \times 10^{-11} M_\odot \text{ yr}^{-1}$ (Chanmugam, Ray, & Singh 1991; Warner 1995), whereas the IPs accrete rapidly, Warner (1995) estimates $\dot{M} \approx (0.2\text{--}4) \times 10^{-9} M_\odot \text{ yr}^{-1}$ from X-ray fluxes of ten systems. Wickramasinghe & Wu (1994) propose that the low accretion rate of AM Hers is a direct consequence of the strong magnetic field of the white dwarf, which inhibits magnetic braking by reducing the number of open field lines along which the magnetized wind from the secondary may flow (for example, see Li, Wickramasinghe, & Wu 1995).

Figure 10 shows the orbital period distributions of known AM Hers and IPs. Most AM Her systems have $P_{\text{orb}} \lesssim 3$ hours, whereas most IPs have $P_{\text{orb}} \approx 3$ –6 hours. This difference has led many to suggest an evolutionary link between the two classes, namely that the asynchronous IPs are the progenitors of the synchronous AM Her systems. For a magnetic field $B \sim 10^7$ G, the magnetospheric radius equals the orbital separation at $P_{\text{orb}} \approx 4$ hrs, suggesting a natural dividing line between synchronous and asynchronous systems (Chanmugam & Ray 1984; King, Frank, & Ritter 1985; Hameury et al. 1987). However, an evolutionary connection is difficult if the white dwarf magnetic field is constant with time. It requires either (i) the IPs and AM Hers have similar magnetic field strengths, but the optical polarization is somehow suppressed in asynchronous rotators, or (ii) the IPs have weaker fields than the AM Her systems, implying a yet to be detected population of asynchronous AM Her progenitors (King & Lasota 1991).

It is striking that the mean accretion rate of the IPs is $> \dot{M}_c$, whereas the AM Her systems accrete at rates $< \dot{M}_c$. Thus, given our results, a natural suggestion is that the magnetic fields of the intermediate polars are low because of the direct effects of the accretion flow. If so, it is possible for an intermediate polar to evolve into an AM Her system if the mass transfer rate drops from $> \dot{M}_c$ to $< \dot{M}_c$ at an orbital period $\approx (3\text{--}4)$ hours (between the observed AM Her and intermediate polar populations).

The reason for such a change in accretion rate is not clear, but is reminiscent of the need for a rapid drop in mass transfer rate to explain the period gap ($P_{\text{orb}} \approx 2$ –3 hours) in non-magnetic CVs. Whether or not the magnetic CVs exhibit a period gap is unclear, there are certainly a higher fraction of magnetic systems in the gap than for non-magnetic systems (King 1994; Kolb 1995; Wheatley 1995). It is however possible that a similar mechanism is operating in both cases, perhaps disrupted magnetic braking, as preferred

for non-magnetic systems (Rappaport, Verbunt & Joss 1983; Howell, Nelson, & Rappaport 2001).

There is an alternative scenario along the same lines as that of Wickramasinghe & Wu (1994). The ROSAT detection of IPs with soft X-ray spectra similar to weaker field AM Hers (Haberl & Motch 1995) has led to suggestions of two populations of IPs. A possibility is that those IPs with fields close to 10^7 G come into synchronous rotation at $P_{\text{orb}} \approx 4$ hours, which causes a drop in \dot{M} as suggested by Wickramasinghe & Wu (1994), allowing the field to subsequently grow to values $\sim 10^8$ G typical of AM Hers. A problem with this picture is what happens to the weaker field IPs (i.e., those with traditional hard X-ray spectra), since very few of them are seen at short orbital periods.

The timescale for reemergence of the field is set by the ohmic diffusion time at the base of the accreted layer. Figure 4 and equation (16) show that this is $\approx 3 \times 10^8$ years $(\Delta M / 0.1 M_{\odot})^{7/5}$ where ΔM is the accreted mass. This is similar to the time for a non-magnetic CV to cross the period gap (Howell et al. 2001). Thus if the drop in mass accretion rate causes the secondary to lose contact with the Roche lobe, there may be time for the field to reemerge before contact is resumed. The impact of any gap on the observed orbital period distribution depends on how strongly the transition orbital period depends on mass transfer rate and magnetic field. With or without a period gap, the lack of known synchronous low field systems could constrain the timescale for reemergence and therefore accreted mass³.

A detailed test of either scenario requires comparison of evolutionary studies and the observed populations of IPs and AM Hers. We note that whereas there is a clear difference in orbital periods and magnetic field strengths between AM Hers and IPs as classes of objects, no correlation is observed between magnetic field strength and orbital period amongst AM Her systems only (WF).

5.2 Where are the 10^9 G accreting WDs?

The highest measured magnetic field in an accreting system is 2.3×10^8 G for AR Uma, whereas the highest observed fields in isolated WDs are close to 10^9 G. Whether or not this difference is significant remains to be seen. For example, WF argue that the very high field accreting white dwarfs have not yet been discovered because of selection effects. There have been suggestions as to why the observed upper limit might differ. Wickramasinghe & Wu (1994) argue that because the high field systems come into synchronization at wider separation, magnetic braking is suppressed earlier, and they do not have time to evolve via gravitational radiation into contact (thus they predict a population of high field, detached binaries).

We would like to point out that some difference would be expected simply because of the different ohmic decay properties of the two populations. The liquid accreting white dwarfs decay at a faster rate than the isolated white dwarfs, which form a solid core after $\sim 10^9$ years of cooling, effectively switching off ohmic decay. To find the maximum difference between the two populations, we assume the isolated white dwarfs undergo no magnetic field decay. The

contrast in field strengths is then $\exp(t/\tau)$, where τ is the decay time. For $\tau = 10^{10}$ years, this gives a factor of 2 after $t = 7$ billion years. This is smaller than the observed factor of ≈ 3 , but should be taken into account when comparing the maximum field strengths of the two populations.

5.3 Type Ia progenitor systems

Currently favoured models for Type Ia supernovae progenitors are rapidly accreting ($\dot{M} \gtrsim 10^{-7} M_{\odot} \text{ yr}^{-1}$), near-Chandrasekhar mass white dwarfs, for example those observed in supersoft X-ray sources or symbiotic binaries. In this case, we would expect amplification of the magnetic field as the central density increases due to accretion ($B \propto \rho^{2/3}$; see §4.2). This amplification is shown in Figure 5 for accretion onto a $0.6 M_{\odot}$ white dwarf, and would be even greater for a massive white dwarf. The density increases especially quickly as you approach Chandrasekhar mass and the electrons become more relativistic, as pointed out by work on compressional heating (Nomoto 1982; Townsley & Bildsten 2001). An important problem is to understand the role played by such an amplified magnetic field in the approach to and evolution after ignition of a Type Ia supernova. For example, Ghezzi et al. (2001), recently pointed out that a large scale magnetic field of 10^8 – 10^9 G can generate asymmetries in the thermonuclear flame front that engulfs the white dwarf during the supernova. Our results show that the prior evolution of the field during accretion should be taken into account.

5.4 Complexity as a result of accretion

Both isolated and accreting white dwarfs often show a complex magnetic field geometry, requiring a significant quadrupole component or an offset dipole (WF). In §2, we found decay times of $(4\text{--}6) \times 10^9$ years for the $l = 2$ decay mode of liquid white dwarfs. Thus one possibility is that the quadrupole field is fossil, requiring that the dipole and quadrupole fields had comparable magnitudes initially.

In isolated systems, the liquid decay time is relevant only for the first $\sim 10^9$ yrs, after which the formation of a solid core increases the ohmic time. Muslimov et al. (1995) studied the Hall effect in isolated white dwarfs as a possible mechanism for generating field complexity as the white dwarf cools. However, the Hall effect is not expected to play a significant role for a liquid interior (Muslimov et al. 1995).

Another possibility is that the accretion flow directly leads to complexity of the field. The spreading of material away from the polar cap (which we have not included in our models in this paper) could induce higher order components of the surface field. An interesting observation is that the magnetic pole undergoing most accretion in AM Her systems is the pole with the weaker magnetic field in all cases with magnetic field measurements for both poles (WF). Wickramasinghe & Wu (1991) suggest that this is a result of the role of the quadrupole component during synchronisation. An alternative suggested by our results is that after synchronisation occurs, the pole pointing towards the companion undergoes more rapid accretion which reduces the field strength at that pole, giving rise to the observed asymmetry. Even though the global rate for AM Hers is $< \dot{M}_c$, the local

³ We thank the referee, J.-M. Hameury, for bringing up this issue.

accretion rate in the layers for which the accreted material is still confined to the polar cap will be greater than the critical rate. Detailed models of the spreading of material away from the polar cap are required to investigate this further.

6 CONCLUSIONS

We have studied the evolution of the magnetic field in an accreting white dwarf. Previous studies of ohmic decay in isolated white dwarfs showed that the ohmic decay time is always longer than the cooling time because the white dwarf develops a solid core. In §2, we calculated the ohmic decay times for the lowest order modes of accreting white dwarfs, which have a liquid interior because of compressional heating by accretion. We found that the lowest order ohmic decay time is $(8\text{--}12) \times 10^9$ yrs for a dipole field, and $(4\text{--}6) \times 10^9$ yrs for a quadrupole field (see Table 1), in good agreement with the earlier calculations of WVS. The difference in ohmic decay times between isolated and accreting white dwarfs should be taken into account when comparing the maximum field strengths of the two populations. In addition, the decay timescale for the quadrupole is long enough that observed quadrupole components (see WF for a summary of the observations) in both accreting and isolated white dwarfs may be fossil if the quadrupole is initially of similar strength to the dipole component.

In §3, we compared the timescale for ohmic decay with accretion, and showed that accretion occurs more rapidly than ohmic diffusion for accretion rates greater than the critical rate $\dot{M}_c \approx (1\text{--}5) \times 10^{-10} M_\odot \text{ yr}^{-1}$. In §4, we calculated the time evolution of the magnetic field as a function of accretion rate, assuming the white dwarf mass increases with time. For a simplified field and accretion geometry (an axisymmetric poloidal magnetic field and spherical accretion), we found that accretion at rates $\dot{M} > \dot{M}_c$ leads to a reduction in the field strength at the surface, as the field is advected into the interior by the accretion flow.

The main conclusion of this paper is that, due to the direct action of accretion, significant changes in the surface magnetic field of an accreting white dwarf could occur during its accretion lifetime. In §5, we showed that accretion induced magnetic field evolution may explain several features of observed systems. Most striking is that the strongly magnetic ($B \sim 10^7\text{--}3 \times 10^8$ G) AM Her systems have a mean accretion rate $\approx 5 \times 10^{-11} M_\odot \text{ yr}^{-1} < \dot{M}_c$ whereas the weakly magnetic ($B \sim 10^5\text{--}10^7$ G) IPs accrete at rates $\sim 10^{-9} M_\odot \text{ yr}^{-1} > \dot{M}_c$. This raises the possibility that the white dwarfs in IPs have subsurface fields as strong as those in AM Hers. If so, this allows for an evolutionary connection between the long orbital period ($P_{\text{orb}} \approx 3\text{--}6$ hours) IPs and short orbital period AM Hers ($P_{\text{orb}} \lesssim 3$ hours), requiring that evolution in orbital period somehow causes a drop in accretion rate (for example, by disrupted magnetic braking as postulated for non-magnetic CVs; see §5.1 for further discussion). The magnetic field would then reemerge on a timescale set by ohmic diffusion, $\approx 3 \times 10^8$ yrs ($\Delta M/0.1 M_\odot$), where ΔM is the accreted mass. Evolutionary calculations are necessary to compare this scenario with the properties of observed systems. We did not consider non-magnetic accreting systems in §5; however, it is possible that many non-magnetic white dwarfs (meaning $B \lesssim 10^5$ G so that the

accretion flow is not disrupted) have submerged magnetic fields if they are accreting at rates $> \dot{M}_c$.

The models presented in this paper are simplified, and many outstanding theoretical questions remain. The major uncertainty in the evolution of accreting white dwarfs is whether the white dwarf mass increases or decreases with time. Even if the mass is increasing with time as we have assumed here, classical nova explosions eject some mass from the system; the effective mass accretion rate is therefore less than the mass transfer rate from the secondary by some factor, introducing an extra uncertainty. If classical novae eject more mass than accreted prior to the thermal runaway, excavation of the white dwarf core leads to a decreasing mass with time. This raises the possibility that the surface magnetic field could grow with time if underlying magnetic field is exposed as the mass decreases. This was originally suggested as a source for the magnetic field of DQ Her by Lamb (1974). Interestingly, this alternative is also consistent with an evolutionary link between AM Hers and intermediate polars, since the magnetic field would increase as the orbital period decreases and successive nova explosions occur. The evolution of the magnetic field under the action of mass loss is left to a future study. The result is presumably somewhat dependent on the initial choice for the current distribution, and differences in the thermal evolution will have to be taken into account.

It is important to understand the spreading of matter away from the polar cap. This topic has received little attention, and is not well-understood. Studies of the polar cap of accreting neutron stars (Hameury et al. 1983; Brown & Bildsten 1998; Litwin, Brown, & Rosner 2001) and white dwarfs (Livio 1983; Hameury & Lasota 1985) suggest that spreading occurs once the sideways force due to the hydrostatic overpressure overcomes the confining magnetic tension, or sooner if instabilities play a role (Litwin et al. 2001). Understanding the spreading process, and its affect on the magnetic field geometry in the outermost layers of the star is directly relevant for interpreting observations of polar cap fields of AM Hers.

Finally, we have not discussed the effect of white dwarf rotation. As mentioned in the introduction, King (1985), applying the results of Moss (1979) to accreting white dwarfs, suggested that meridional currents could be responsible for the submergence of magnetic flux in the outer layers of rotating magnetic white dwarfs. The aim was to explain the narrow range of field strengths in AM Hers. The effect of meridional flows in accreting white dwarfs deserves further investigation.

ACKNOWLEDGMENTS

We thank Dayal Wickramasinghe for conversations about observations of magnetic white dwarfs, and Graham Wynn for emphasising the lack of very strongly magnetic accreting white dwarfs. We are grateful to Ellen Zweibel for discussions about the appropriate surface boundary conditions in our global models, and to the referee Jean-Marie Hameury for carefully questioning our assumptions and conclusions. We thank Hugh van Horn for communications regarding earlier work, Phil Arras and Chris Thompson for discussions about the Hall effect, and Dean Townsley and Lars Bildsten

for discussions about their models of compressional heating. We acknowledge support from NASA through Hubble Fellowship grant HF-01138 awarded by the Space Telescope Science Institute, which is operated by the Association of Universities for Research in Astronomy, Inc., for NASA, under contract NAS 5-26555.

APPENDIX A: ELECTRICAL CONDUCTIVITY FOR ARBITRARY DEGENERACY

In the white dwarf envelope, the electrons go from being non-degenerate to degenerate. Hubbard & Lampe (1969) calculated the thermal conductivity for arbitrary degeneracy, presenting their results in tabulated form. Unfortunately, other calculations of conductivity which present their results in terms of fitting formulae, such as those of Yakovlev & Urpin (1980) and Itoh et al. (1983) are for degenerate electrons only (for thermal conductivity, this is the regime of interest, since radiative heat transport dominates at low densities). In their study of ohmic decay in cooling white dwarfs, WVS adopted an interpolation scheme between calculations in the different regimes. We have taken a different approach, which we now describe.

For non-relativistic electrons, the density and electrical conductivity may be written

$$n_e = \frac{\sqrt{2}(m_e k_B T)^{3/2}}{\pi^2 \hbar^3} F_{1/2}(\alpha) \quad (\text{A1})$$

and

$$\sigma = \frac{2m_e (k_B T)^3}{\pi^3 \hbar^3 \Lambda_{ei} Z n_e e^2} F_2(\alpha), \quad (\text{A2})$$

where $\alpha = -(E_F - m_e c^2)/k_B T$, and the Fermi integrals $F_n(\eta)$ are given by

$$F_n(\alpha) = \int_0^\infty \frac{x^n dx}{1 + \exp(x + \alpha)}. \quad (\text{A3})$$

In equation (A2), we assume the Coulomb logarithm Λ_{ei} varies slowly enough with electron energy that it may be taken out of the integral. For degenerate electrons, $\alpha \ll -1$, equation (A2) reduces to the small x (non-relativistic) limit of equation (3). For non-degenerate electrons, $\alpha \gg 1$, equation (A2) reduces to equation (19) (Spitzer 1962).

Our approach in this paper is to evaluate σ using equation (A2), with Λ_{ei} a function of density, and with a correction for relativistic effects. We evaluate the Fermi integral $F_2(\alpha)$ by direct numerical integration. The electron number density is used to determine α , by inverting equation (A1) using the fit of Antia (1993) to the inverse of $F_{1/2}$.

We calculate the Coulomb logarithm as a function of density by interpolating between the non-degenerate result of Spitzer (1962) and the degenerate results of Yakovlev & Urpin (1980). We adopt the expression of Yakovlev & Urpin (1980) for the Coulomb logarithm, but rewrite it in terms of the electron momentum, choosing x in such a way that in the non-degenerate limit, we obtain Spitzer's formula. The Coulomb logarithm is $\Lambda_{ei} = \Lambda_{ei}^{(0)} - v^2/2c^2$, where $\Lambda_{ei}^{(0)} = \ln(r_{\max}/r_{\min})$ (YU). Here r_{\min} and r_{\max} are the limits of the integral over impact parameters. For temperatures greater than 4.2×10^5 K (Spitzer 1962), r_{\min} is set by the de Broglie wavelength of the electrons, we take

$r_{\min} = \hbar/2p_e$. The cutoff r_{\max} is set either by the Debye length, given by $r_D^2 = m_p k_B T / 4\pi e^2 \rho \sum Y_i Z_i^2$, or the interior spacing $a = (3/4\pi n_i)^{1/3}$, whichever is larger. We obtain

$$\begin{aligned} \Lambda_{ei}^{(0)} &= \ln \left[\left(\frac{2}{9\pi} \right)^{1/3} \frac{m_e c}{\hbar} \frac{x}{(\sum n_i)^{1/3}} \left(\frac{3}{\Gamma} + \frac{3}{2} \right)^{1/2} \right] \\ &= \ln \left[\frac{127 x}{\rho^{1/3} (\sum Y_i)^{1/3}} \left(\frac{3}{\Gamma} + \frac{3}{2} \right)^{1/2} \right] \end{aligned} \quad (\text{A4})$$

where

$$\Gamma = \frac{e^2}{k_B T a} \frac{\sum n_i Z_i^2}{\sum n_i} = 0.11 \left(\frac{\sum_i Y_i Z_i^2}{\sum_i Y_i} \right) \frac{(\rho_5 \sum_i Y_i)^{1/3}}{T_8}, \quad (\text{A5})$$

(Hubbard & Lampe 1969; $\Gamma = (1/3)(a/r_D)^2$), and where $x = (x_1^2 + x_2^2)^{1/2}$, with $x_2 = (3k_B T/m_e c^2)^{1/2} = 0.22 T_8^{1/2}$.

Finally, we include a correction for relativistic effects. Because we use equation (A1) to solve for α , we obtain the non-relativistic value for α in the degenerate limit, and equation (A2) reduces to the small x limit of equation (3). To include relativistic effects, we divide equation (A2) by a factor $1 + x^2$, so that we recover equation (3) in full in the degenerate limit.

For the $T = 0$ models of §2 and §4, we write out $\Lambda_{ei}^{(0)}$ as a sum of logarithmic terms, but drop the term containing the temperature T , which contributes $< 10\%$ to the final value of Λ_{ei} .

REFERENCES

- Antia H. M., 1993, ApJS, 84, 101
Baiko D. A., Yakovlev D. G., 1995, Ast. Lett., 21, 702
Bhattacharya D., 1995, in X-Ray Binaries, ed. W. H. G. Lewin, J. van Paradijs, & E. P. J. van den Heuvel (Cambridge: Cambridge University Press), 233
Bonnet-Bidaud J. M., Mouchet M., de Martino D., Matt G., Motch C., 2001, A&A, 374, 1003
Brown E. F., Bildsten L., 1998, ApJ, 496, 915
Chakrabarty D., Morgan E. H., 1998, Nature, 394, 346
Chanmugam G., Gabriel M., 1972, A&A, 16, 149
Chanmugam G., Ray A., 1984, ApJ, 285, 252
Chanmugam G., Ray A., Singh K. P., 1991, ApJ, 375, 600
Choudhuri A. R., Konar S., 2001, submitted to MNRAS (astro-ph/0108229)
Cumming A., Zweibel E., Bildsten L., 2001, ApJ, 557, 958 (CZB)
Farouki R. T., Hamaguchi S., 1993, Phys. Rev. E, 47, 4330
Fontaine G., Thomas J. H., van Horn H. M., 1973, ApJ, 184, 911
Fujimoto, M. Y. 1982, ApJ, 257, 767
Ghezzi C. R., de Gouveia Dal Pino E. M., Horvath J. E., 2001, ApJ, 548, L193
Goldreich P., Reisenegger A., 1992, ApJ, 395, 250
Haberl F., Motch C., 1995, A&A, 297, L37
Hameury J. M., Lasota J. P., 1985, A&A, 145, L10
Hameury J. M., Bonazzola S., Heyvaerts J., Lasota J. P., 1983, A&A, 128, 369
Hameury J. M., King A. R., Lasota J. P., Ritter H., 1987, ApJ, 316, 275
Howell S. B., Nelson L. A., Rappaport S., 2001, ApJ, 550, 897
Hubbard W. B., Lampe M., 1969, ApJS, 18, 297
Itoh N., Mitake S., Iyetomi H., Ichimaru S., 1983, ApJ, 273, 774
King A. R., 1985, MNRAS, 217, 23P
King A. R., Frank J., Ritter H., 1985, MNRAS, 213, 181
Lamb D. Q., 1974, ApJ, 192, L129
Lamb D. Q., Patterson J., 1983, in IAU Colloquium 72, Variables

- and Related Objects, ed. M. Livio, and G. Shaviv (Dordrecht: Reidel), p. 299
- Li J., Wickramasinghe D. T., Wu K., 1995, MNRAS, 276, 255
- Litwin C., Brown E. F., Rosner R., 2001, ApJ, 553, 788
- Livio M., 1983, A&A, 121, L7
- Livio M., 1995, in ASP Conf. Ser. 85, Magnetic Cataclysmic Variables, ed. D. A. H. Buckley, & B. Warner (Astronomical Society of the Pacific: San Francisco), 80
- Livio M., Shankar A., Truran J. W., 1988, ApJ, 330, 264
- Livio M., Truran J. W., 1992, ApJ, 389, 695
- MacDonald, J. 1983, ApJ, 267, 732
- Mestel L., 1999, Stellar Magnetism (Oxford: Oxford University Press)
- Moss D., 1979, MNRAS, 187, 601
- Muslimov A. G., van Horn H. M., Wood M. A., 1995, ApJ, 442, 758 (MVW)
- Nomoto K., 1982, ApJ, 253, 798
- Press W. H., Teukolsky S. A., Vetterling W. T., Flannery B. P., 1992, Numerical Recipes: The Art of Scientific Computing (2d ed.; New York: Cambridge Univ. Press)
- Rappaport S., Verbunt F., & Joss P. C., 1983, ApJ, 275, 713
- Ritter H., Kolb U., 1998, A&AS, 129, 83
- Romani R. W., 1990, Nature, 347, 741
- Romani R. W., 1995, in Millisecond Pulsars, A Decade of Surprise, ASP Conference Series, Volume 72, ed. A.S. Fruchter, M. Tavani, & D.C. Backer (Astronomical Society of the Pacific: San Francisco), 288
- Schatz H., Bildsten L., Cumming A., Wiescher M., 1999, ApJ, 524, 1014
- Spitzer L. Jr., 1962, Physics of Fully-Ionized Gases (New York: Wiley)
- Townsley D. M., Bildsten L., 2001 in ASP Conf. Ser. XX, The Physics of Cataclysmic Variables and Related Objects, ed. B. T. Gänsicke, K. Beuermann, & K. Reinsch (San Francisco: ASP), XXX
- Warner B., 1995, Cataclysmic Variable Stars (Cambridge: Cambridge University Press)
- Wendell C. E., van Horn H. M., Sargent D., 1987, ApJ, 313, 284 (WVS)
- Wickramasinghe D. T., Ferrario L., 2000, PASP, 112, 873 (WF)
- Wickramasinghe D. T., Wu K., 1994, MNRAS, 266, L1
- Wijnands R., van der Klis M., 1998, Nature, 394, 344
- Wu K., Wickramasinghe D. T., 1993, MNRAS, 265, 115
- Yakovlev D. G., Urpin V. A., 1980, Soviet Astron, 24, 303